Status of the RICE Experiment

Dave Besson, KU Physics Dept., Lawrence, KS 66045-2151

Abstract. The RICE experiment (Radio Ice Čerenkov Experiment) at the South Pole, currently one of the projects included in the overall AMANDA effort, seeks to measure ultra-high energy electron neutrinos ($E_\nu > 10^{15}$) by detection of the long-wavelength Čerenkov Radiation (CR) signal resulting from neutrino-induced showers: $\nu_e + N \to e + N'$. We present upper limits on the UHE ν_e flux based on analysis of August, 2000 data.

RICE concept and current experimental configuration: The RICE[1] experiment is similar to the primary AMANDA effort in that it seeks to measure ultra-high energy (UHE) neutrinos by detection of Čerenkov radiation resulting from the collision of a UHE neutrino with the target ice.

The RICE concept is illustrated in Figure 1, depicting a Čerenkov cone fit to a set of "struck" dipole receivers in one particular event, along with the extracted neutrino direction. High amplitude/early time receivers are indicated by the shading/icon-size scheme. In the actual array geometry, dipole receivers are spread over a 200 m $\times$ 200 m $\times$ 200 m cube beneath and around the Martin A. Pomerantz Observatory (MAPO), approximately 1 km. from the geographic South Pole.

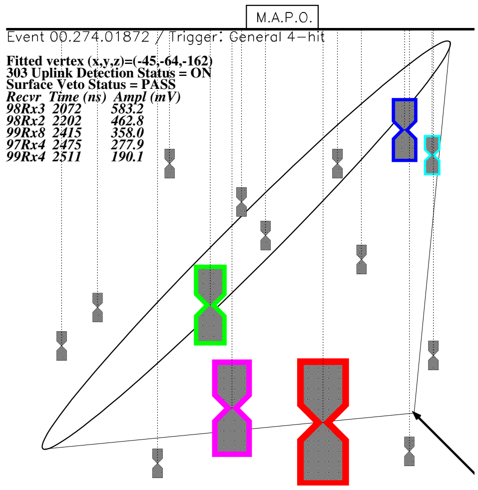

FIGURE 1.: Sample RICE event.

Whereas AMANDA is optimized for detection of penetrating muons compact resulting from $\nu_\mu + N \to \mu + N'$, RICE seeks to measure electromagnetic cascades initiated by electrons or positrons:

---

1) RICE includes: Dave Seckel and Glenn Spiczak (Bartol Research Institute, Newark DE), Jenni Adams (U. of Canterbury, Christchurch, NZ), George M. Frichter (Florida State University, Tallahassee FL) Chris Allen, Alice Bean, Dave Besson, DJ Box, Roman Buniy, Eben Copple, Ryan Dyer, Doug McKay, John Ralston, Soeb Razzaque, Surujhedo Seunarine, Dave Schmitz (University of Kansas, Lawrence KS), and Ilya Kravchenko (M.I.T., Cambridge, MA), and is supported by The Research Corporation, NSF EPSCoR, the University of Kansas, The Marsden Foundation, and the NSF OPP and EPP Divisions.

$\nu_e + N \rightarrow e + N'$. As the cascade develops, atomic electrons in the target medium are swept into the forward-moving shower, resulting in a net charge on the shower front of $Q_{tot} \sim 0.25 E_s(GeV)e$.

Such cascades produce broadband Čerenkov radiation – for wavelengths larger than the transverse dimensions of the shower front ($2r_{Moliere}$, or $\approx$10 cm in ice), the emitting region increasingly approximates a line charge of magnitude Q_{tot}. At these (RF) wavelengths, the net Čerenkov radiation produced by the shower front can therefore be considered coherent. By contrast, the resultant short wavelength (optical frequency) Čerenkov power is obtained from an incoherent sum over the electric field vectors associated with each short-wavelength Čerenkov wavefront. The experimental sensitivity in the RF regime is further enhanced by the high transparency of cold polar ice ($\lambda^{1\ GHz}_{atten}$ $\sim$1 km). One analysis [1] indicates that a radio receiver offers greater sensitive volume per module than photomultiplier tubes for 1 PeV$< E_{\nu_e}$.

The RICE experiment presently includes 18 half-wave dipole receivers underice, deployed over the period 1996-1999. Receivers have good reception characteristics over the range 0-1 GHz. Also deployed are three large TEM surface horn antennas which are used as a veto of surface-generated noise. Whenever one of the surface horns registers a signal that exceeds threshold, data-taking is inhibited for the subsequent 3.5 μsec. The signal from each underice antenna is boosted by a 36-dB in-ice amplifier, then carried by coaxial cable to the surface observatory, where the signal is filtered (suppressing noise below 200 MHz), re-amplified (either 52 dB or 60 dB), and split into two copies. One copy is fed into a CAMAC crate; after initial discrimination (using a LeCroy 3412E discriminator), the signal is routed into a NIM crate where the trigger logic resides. The other signal copy is passed to the input of an HP54542 digital oscilloscope where waveform information is buffered and recorded.

The status of the current array deployment is summarized in Figure 2. Indicated in the figure are the AMANDA holes (1-19, drilled using the hot-water technique) containing RICE receivers, and also the four holes drilled specifically for RICE in 1998-99 (using a mechanical drill) containing RICE-only equipment. All channels (receiver "Rx" or transmitter "Tx") are indicated by a 5-character alphanumeric string corresponding to the year of deployment, the type of dipole antenna deployed, and a numerical identifier. Also indicated on the Figure is the MAPO building which houses the RICE (and AMANDA) surface electronics. The AMANDA array is located approximately 600 m (AMANDA-A) to 1400 m (AMANDA-B) below the RICE array in the ice; the SPASE experiment is located approximately at $x \sim -400$m on the Figure.

A valid event trigger is defined when any one of three criteria is satisfied in a time window of 1 μs: i) $\geq$4 underice antennas register signals exceeding threshold, ii) $\geq$ one underice antenna registers a signal above threshold in coincidence with a high-amplitude SPASE event, iii) $\geq$ one underice antenna registers a signal above threshold in coincidence with a 30-fold PMT AMANDA trigger. There are two

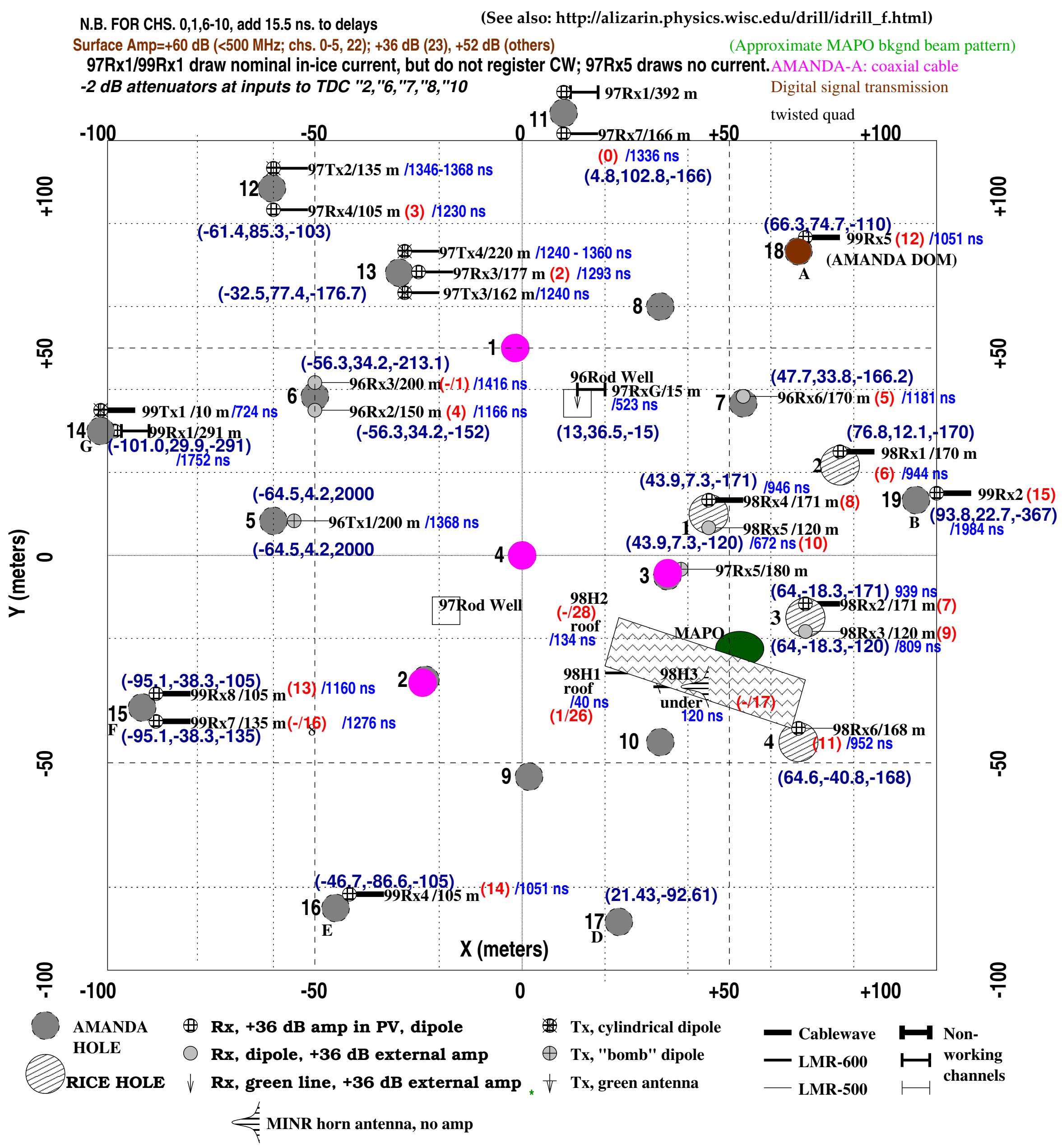

FIGURE 2. Present geometry of the RICE array, relative to AMANDA hole 4. "Tx" designate transmitters; "Rx" desginate receivers. (x,y,z) of receivers and transmitters are shown.

primary ways that surface-generated background transient events can be vetoed – either: a) one of the surface horn antennas registers a signal in coincidence with any of the above three trigger criteria being satisfied, or b) the timing sequence of hits in the underice antennas is determined to be consistent (in software) with the sequence expected from surface generated backgrounds. If any of the above trigger criteria are satisfied and there is no veto signal, the time of each hit above threshold (as recorded by a LeCroy 3377 TDC), and also an 8 μs buffer of data stored in an HP54542 digital oscilloscope at 1 GSa/s (for each channel) is written to disk. Each event is also given a GPS time stamp for synchronization with other South Pole (and more global) experiments. Data is subsequently ftp'ed back to the US for further analysis. Data runs are initiated remotely from the home institutions in the States during the time when there is a satellite connection to the RICE DAQ PC. Raw trigger rates (before veto) are typically 30 Hz; typical data-taking rates after the veto are 0.01 – 0.1 Hz. Experimental sensitivity and data-taking is limited by: a) the time required to write information from the digital scopes to disk (~10 sec/event), b) the time required to perform the surface-background veto in software (~10 msec/event), and c) our inability to take data at those times when the South Pole satellite uplink (broadcast at 303 MHz) is active, due to the high amplitude of the uplink signal. When this uplink is not active, the discriminator thresholds correspond to typical livetimes of ~80%.

A typical surface-generated background event is shown in Figure 3. In the event display, each of the traces corresponds to one of the under-ice antennas. Vertical bars indicate the TDC time recorded for each particular channel; the rise time and timing resolution of each receiver as determined by waveform information is evident from the Figure. This particular event shows receiver -to- receiver timing delays characteristic of surface-generated background noise. As can be seen in the event, leading edge resolution is typically 5-10 nsec; the ring time for each antenna is typically 50 nsec.

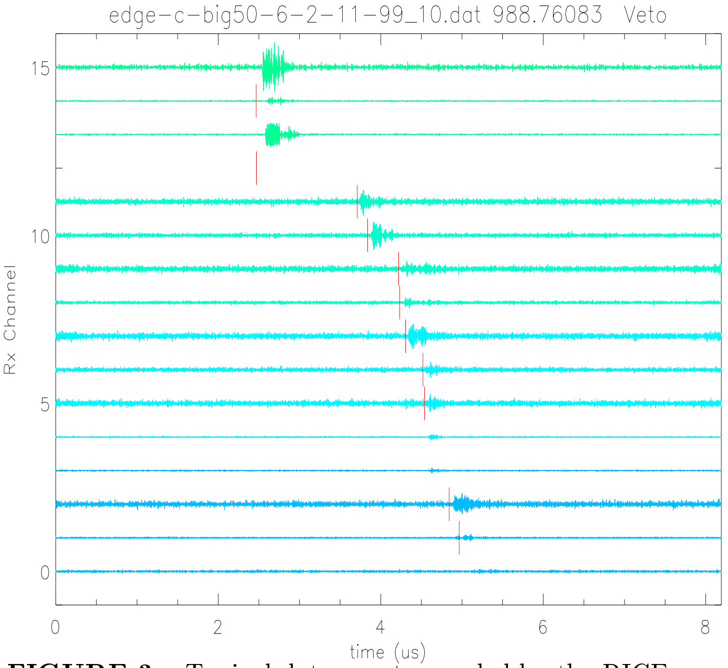

FIGURE 3.: Typical data event recorded by the RICE array.

Expected Detector Performance and Calibration Status:

Expected Angular Resolution: The angular resolution expected for a real neutrino-induced event is determined from Monte Carlo simulations. A ν_e-induced cascade is simulated directly below the radio array, and the Cerenkov cone propagated vertically upwards to the array. Antennas in the simulation are located at 40 m, 80 m, 120 m and 160 m from the event vertex, to correspond to the close-packing of the current array geometry. For the best case in which the Čerenkov cone directly intercepts these four antennas, the corresonding hit times are calculated for each struck antenna, then these times are smeared by 25 ns, to match our experimental timing resolution. Using these smeared times, the cone orientation is numerically calculated and then compared with the true input Čerenkov cone orientation. The deviation in cone orientation corresponds directly to the deviation between the true incident neutrino direction and the calculated incident neutrino direction. The results of the simuation are shown in Figure 4.

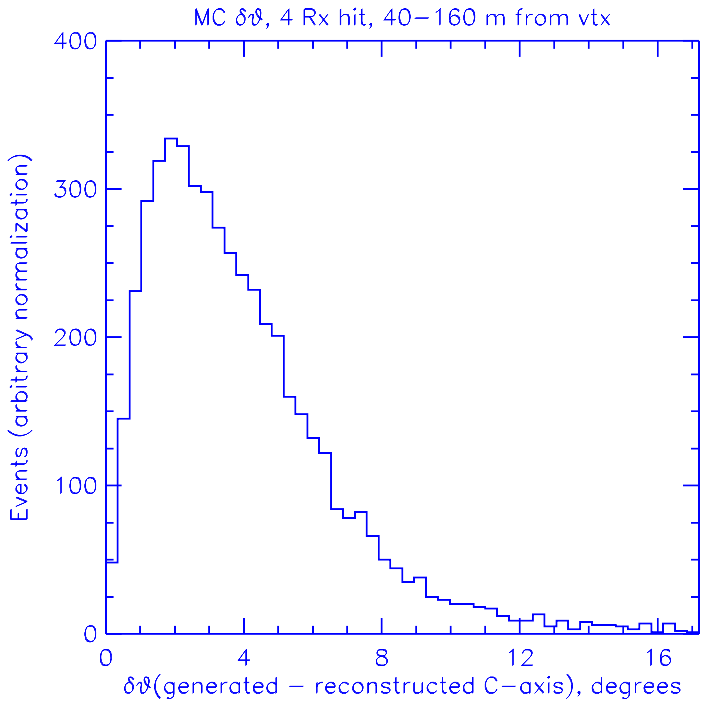

FIGURE 4.: Deviation between reconstructed incident neutrino direction vs. calculated incident neutrino direction, using Monte Carlo simulations.

Typical deviations are of order 4-5 degrees. The simulation is optimistic in that the struck antennas are all considered to be directly on the Čerenkov cone; in reality, the finite width of the Čerenkov cone will smear each hit by an additional degree or so. However, this smearing can be compensated for, to a large extent, by: a) use of amplitude information to deduce how far off the Čerenkov cone angle of 57 degrees a struck antenna is actually located, and b) inclusion of more struck antennas to provide redundancy for the event vertex/neutrino momentum vector calculation.

Timing calibration: Event and source reconstruction is performed by a χ^2 minimization process derived from a knowledge of the relative delays δt_{ij} in the signal arrival times for a given event, in each underice receiver. Given four or more hit antennas (i.e., 3 δt_{ij} values), an event vertex and source direction can be determined numerically. Contributions to δt_{ij} come from several sources, including differences in signal propagation velocity in the ice due to variations in the dielectric constant with depth, differences in signal propagation speed within the different analog cables being used, differences in cable lengths, and channel-to-channel jitter within the surface readout and data acquisition electronics.

Buried transmitters are used to calibrate the channel-to-channel timing delays. A 1 ns duration pulse (comparable to the duration of an expected neutrino-induced event) is sent to one of five buried transmitters, which subsequently broadcasts the signal to the receiver array. An event vertex is reconstructed exclusively from the measured time delays; comparison with the actual transmitter location allows a calculation of the timing residual χ^2 for each channel $(\frac{\delta t_{ij}^{\text{measured}} - \delta t_{ij}^{\text{expected}}}{\sigma_t})^2$. An iterative procedure is used to calibrate out the observed channel-to-channel timing delays and minimize the timing residuals for an ensemble of transmitter events. Typical corrections, per channel, are of order 25 ns. A calibration event is shown in Figure 5. Here the χ^2 probability is calculated over a 3 dimensional grid (grid size = 20m) of possible vertex points 500 meters on a side. Three orthogonal 2 dimensional slices each passing though the minimum value of χ^2 are shown. The shading indicate probabilities ranging from near zero (black) to near unity. Small squares indicate the positions of all RICE receivers and the the white diamond indicates the known position of the RICE transmitter 96Tx1 which emitted the reconstructed pulse. In this case the difference between known and reconstructed event vertex is about 13m. The spatial residual, at this very early level of calibration, is typically 10 meters, which is consistent with the intrinsic resolution of our calibration technique (with more CPU, this can be improved somewhat).

Amplitude Calibration: Amplitude calibration is achieved as follows: a 1 milliwatt (0 dBm) continuous wave (CW) signal is broadcast through the transmit port of an HP8713C network analyzer. The NWA scans through the frequency range 0→1000 MHz in 200 bins, producing a 0 dBm CW signal in each frequency bin. The signal is transmitted through ~1000 feet of coaxial cable to one of the five under-ice dipole transmitting antennas. The transmitters subsequently broadcast to the underice receiver array, and the return signal power (after amplification, passing through cable and being fed back into the return port of the network analyzer) is then measured. Then, using laboratory measurements made at KU of: a) the effective area of the dipole antennas, as a function of frequency, and b) the dipole Tx/Rx efficiency as a function of polar angle and azimuth, c) cable losses and dispersion effects for the various cables used in the RICE experiment, d) the gain of the two stages of amplification as determined from RICE data acquired *in situ* by normalizing to thermal noise, and also correcting for $1/r^2$ spherical spreading of the signal, one can model the receiver array and calculate the expected signal

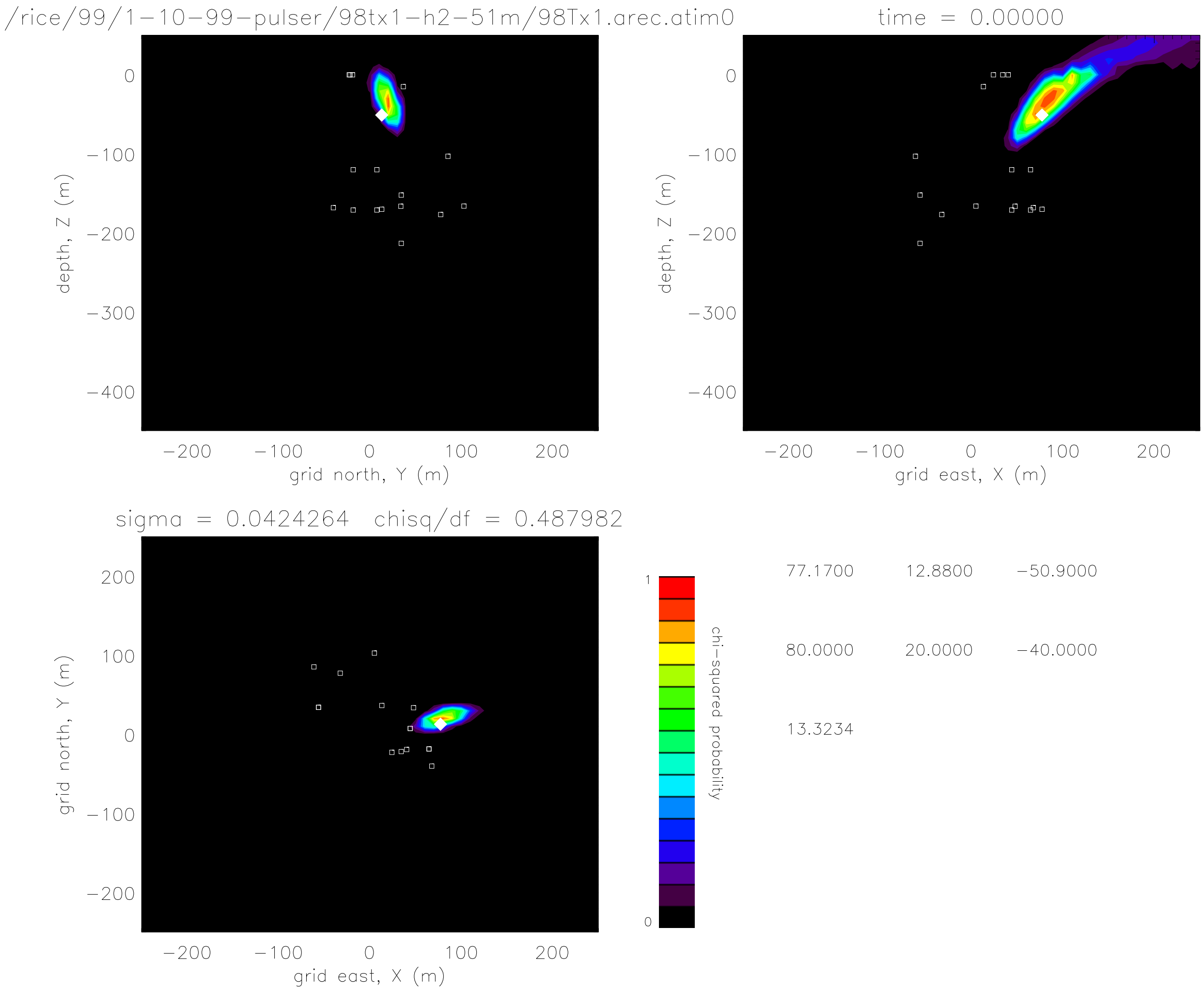

FIGURE 5. Reconstruction of Tx pulse, based exclusively on measured receiver times, shown in the three possible planar slices. Diamond indicates known location of transmitter; shading intensity code indicates χ^2 of reconstruction. Open white squares indicate receivers.

strength returning to the return port of the network analyzer. This can then be directly compared with actual measurement.

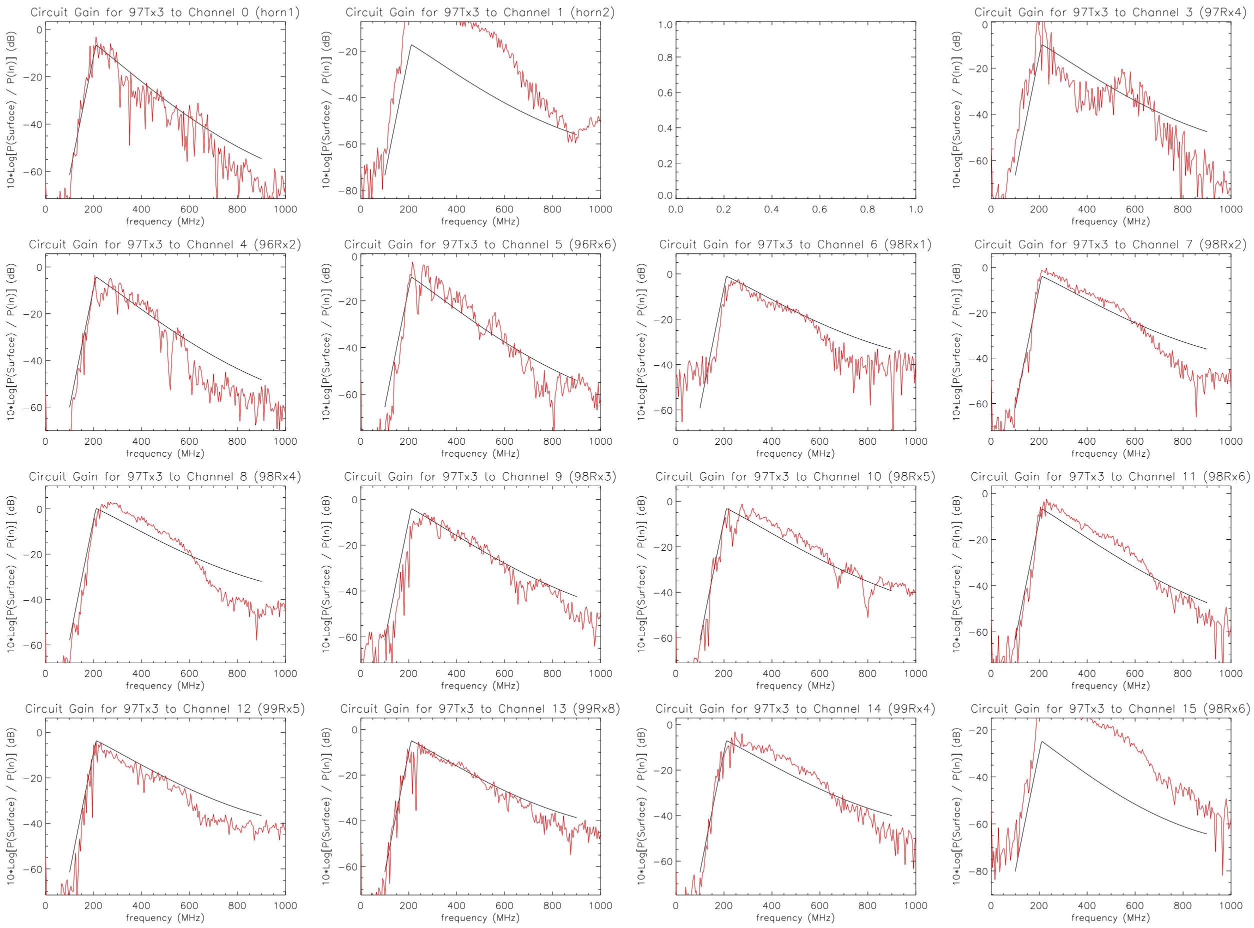

FIGURE 6.: Comparison of expected (solid curve) vs. measured (histogram) Tx→Rx signal strength for one transmitter broadcasting to 16 receivers.

Such a comparison, as a function of frequency, is shown in Figure 6 for one transmitter (97Tx3). With the exception of channels “1 and “15, for which the antenna response is anomalously high, within the “analysis” frequency band of our experiment (200 MHz - 500 MHz), our level of uncertainty in the total circuit power is ±6 dB. Note that, for the case of a neutrino event, this uncertainty can be considered to be conservative, as it folds in effects of both the receiver and the transmitter.

Figure 7 shows the distribution of sources recorded in 15 days of livetime accumulated during August, 2000. The majority of our triggers to date are consistent with either surface-generated noise backgrounds (Z≥0, as shown in the Figure) or random thermal noise hits; no clear neutrino candidates have been observed. Unfortunately, the signal rate expected for other physics processes, given the very high energy experimental threshold and the current configuration, is almost negligible. (For our current array, we expect to observe less than 0.1 hard bremstrahlung from a UHE muon, e.g., in one year.) Given the known discriminator thresholds, and folding in known experimental effects, an effective volume, as a function of incident neutrino energy, can be calculated (Figure 8).

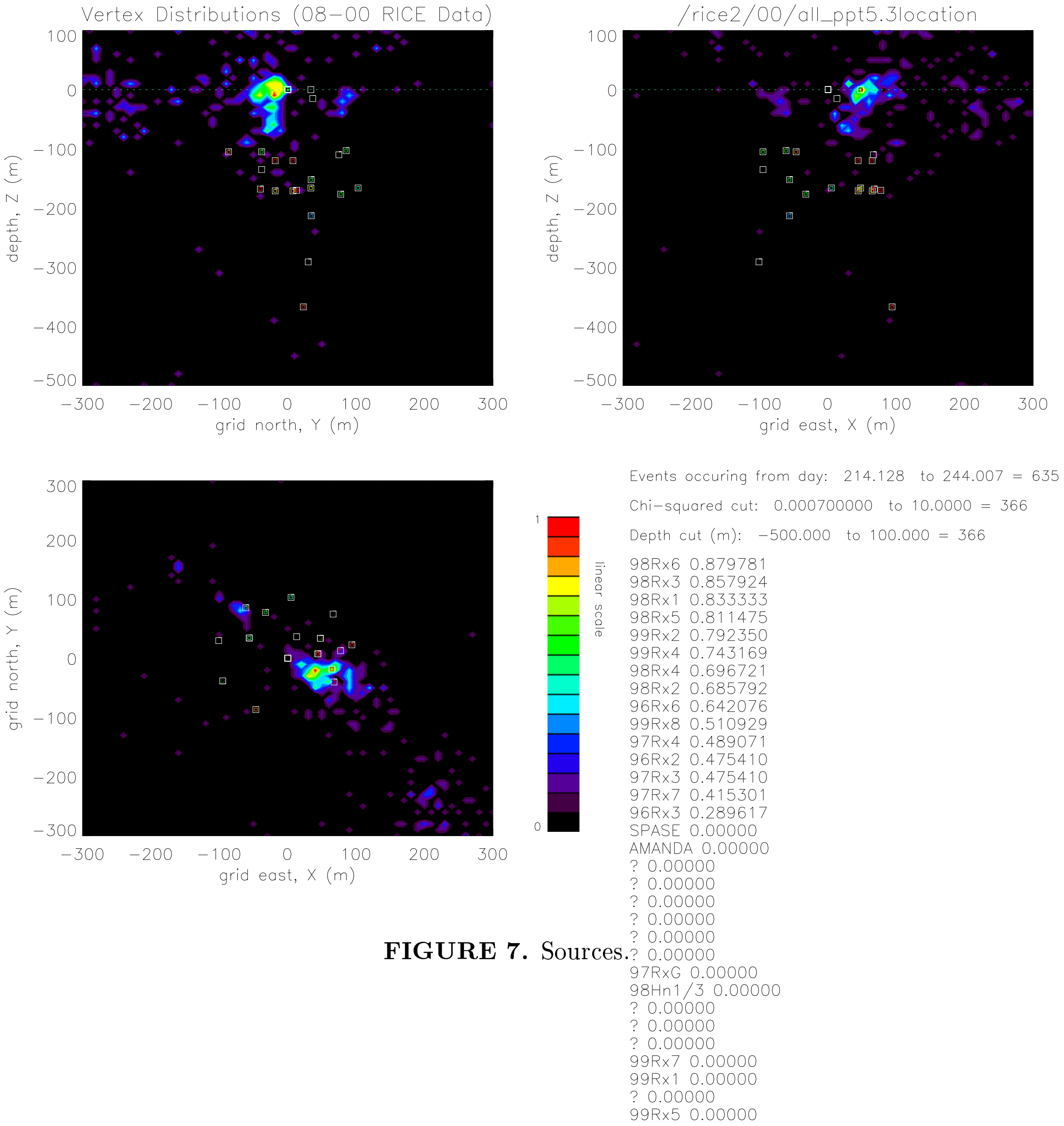

FIGURE 7. Sources.

In the figure, the uppermost black curve corresponds to the effective volume in which only one receiver must be hit, with a discriminator threshold corresponding to thermal noise. The closely spaced curves correspond to more realistic cases requiring n=4, 5, 6... antennas hit, with our current experimental thresholds. The uppermost of the closely-spaced curves (n=4) corresponds to our current experimental configuration.

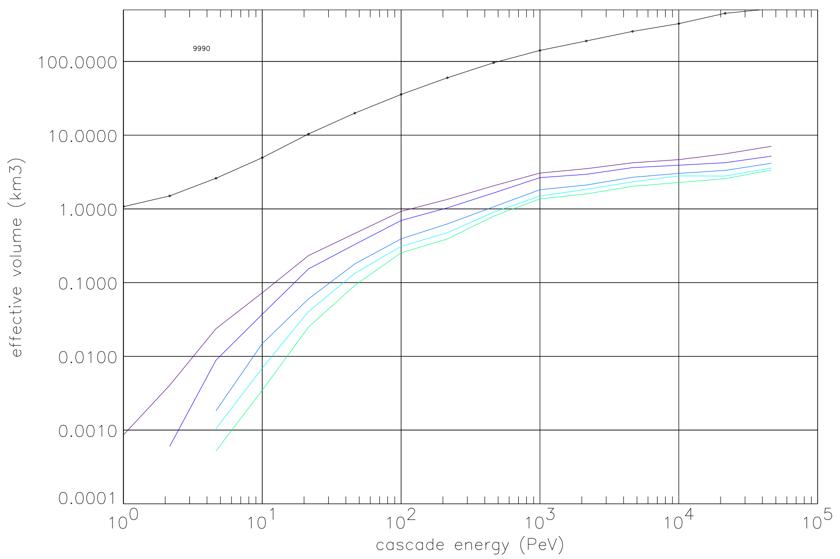

FIGURE 8.: Calculated effective volume, as a function of energy. The curves shown correspond to various assumptions about the experimental thresholds.

Knowing the total livetime, the effective volume, and based on two candidates which have not yet been eliminated, one can then calculate an upper limit on the incident ν_e flux, as a function of incident energy (Figure 9). In the figure, the predictions, shown as solid lines, correspond to (in order of descending flux, as measured at 1 PeV): Stecker & Salamon [2], Protheroe [3], Mannheim (B) [5], Mannheim (A) [4], Yoshida et al. GZK-model [6]. Dashed lines represent our current upper limits for the Stecker & Salamon, Protheroe, and Mannheim (B) models (from left to right), based on analysis of the August, 2000 data only.

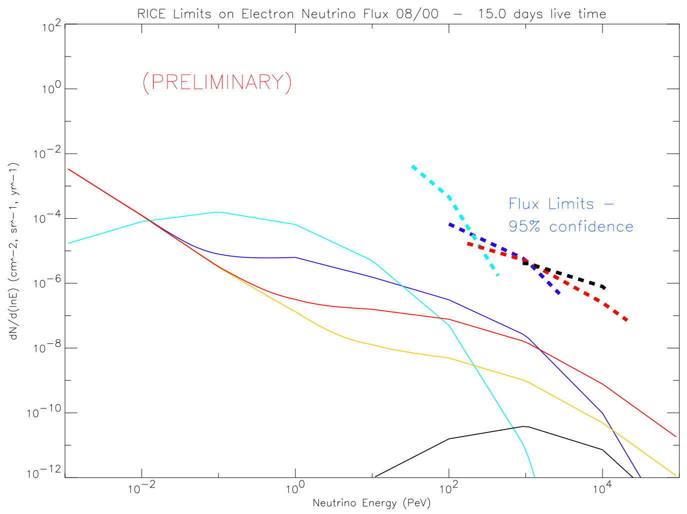

FIGURE 9.: Neutrino flux model predictions (solid) and corresponding RICE calculated upper limits (dashed), as a function of neutrino energy.

Alternately, we can plot our upper limits as a function of the spectral index

γ of the assumed incident neutrino energy spectrum: $dN/dE_\gamma \sim E^{-\gamma}$. These are shown in Figure 10, for a range of γ values. Note that the dashed lines cover the region for which our sensitivity is maximal given the assumed incident neutrino spectrum; the integral under the dashed line corresponds to our upper limit. As the spectral index increases, our sensitivity is pushed to lower and lower energy regions. Again, we have used only August, 2000 data for this analysis. Data taken from Jan., 1999 - Dec., 2000 has yet to be fully analyzed.

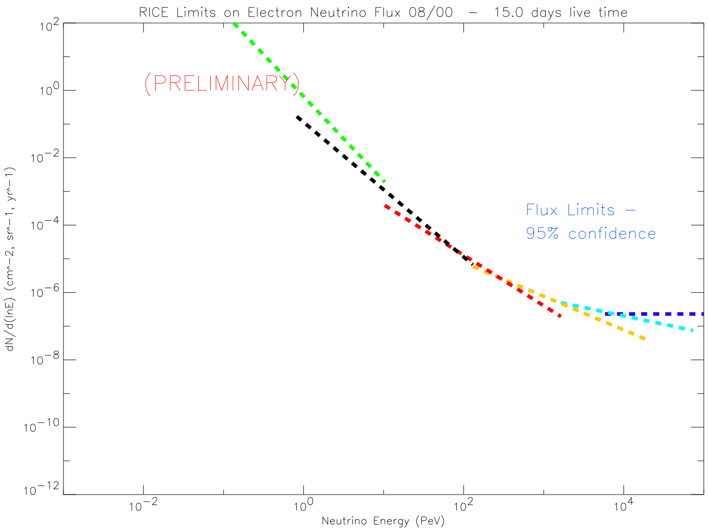

FIGURE 10.: RICE calculated upper limits on neutrino flux assuming $dN/dE \sim E^{-\gamma}$ input spectrum, with the spectral index varying from γ=3.5 to γ=1.0, in increments of $\Delta\gamma$=0.5 (from left to right).

Future Plans Further improvement in the current array can be achieved by: a) deployment of additional receiver modules, b) improvement of signal transmission technology (optical fiber, e.g., over coaxial cable), and c) stronger rejection of surface backgrounds.

Acknowledgments The RICE experiment is supported by the National Science Foundation, the University of Kansas, and the Research Corporation. Special thanks go to the AMANDA Collaboration, Matt Peters of the U. of Texas SOAR group, and the winterovers at South Pole Station.

REFERENCES

1. P.B. Price (UC, Berkeley). **astro-ph/9510119**, 1995, published in Astropart. Phys. 5, 43, 1996.
2. F. W. Stecker and M. H. Salamon, **astro-ph/9501064**
3. A. P. Szabo and R. J. Protheroe, Astropart. Phys. **2**, 375 (1994); R. J. Protheroe and A. P. Szabo, Phys. Rev. Lett. **69**, 2285 (1992).
4. K. Mannheim, astro-ph/9306005, Phys. Rev. D**48** (1993) 2408-2414
5. K. Mannheim, R. Protheroe, and J. Rachen, astro-ph/9812398, and Phys. Rev. D**63** (2001) 023003
6. S. Yoshida, G. Sigl, and S. Lee, hep-ph/9808324, Phys.Rev.Lett. 81 (1998) 5505-5508, and G. Sigl, S. Lee, P. Bhattacharjee, and S. Yoshida, hep-ph/9809242, Phys.Rev. D59 (1999) 043504